Amphiphilic diblock and triblock copolymers based on poly(2-methyl-2-oxazoline) and poly(D,L-lactide): Synthesis, physicochemical characterizations and self-assembly properties

Gaëlle Le Fer, Clémence Le Cœur, Jean-Michel Guigner, Catherine Amiel, Gisèle Volet

Amphiphilic diblock and triblock copolymers based on poly(2-methyl-2-oxazoline) and poly(D,L-lactide): synthesis, physicochemical characterizations and self-assembly properties.

Gaëlle Le Fer[†], Clémence Le Cœur[†§], Jean-Michel Guigner[‖], Catherine Amiel[†], and Gisèle Volet[*†‡]

[†] Université Paris-Est, ICMPE (UMR7182), CNRS, UPEC, 94320 Thiais, France

[‡] Université d'Evry Val d'Essonne, Rue du Père Jarlan, 91025 Evry Cedex, France

[§] Laboratoire Léon Brillouin, UMR 12 CEA–CNRS, CEA Saclay, 91191 Gif-sur-Yvette Cedex, France

[‖] Institut de Minéralogie, de Physique des Matériaux et de Cosmochimie (IMPMC), Sorbonne Universités, UPMC Paris 6, IRD, CNRS UMR7590, MNHN, 4 place Jussieu, 75252 Paris Cedex 05, France

Key-words: poly(2-methyl-2-oxazoline), block copolymers, micelles, Small-Angle Neutron Scattering.

Abstract

A range of amphiphilic diblock and triblock copolymers based on poly(2-methyl-2-oxazoline) (PMeOx) and poly(D,L-lactide) (PLA) with various compositions and molecular masses were prepared combining cationic ring-opening polymerization and click chemistry. Their hydrophilic weight ratios (*f*) covered a wide range of composition (21 to 77 %). In water, these amphiphilic copolymers self-assembled to form, in the case of diblock copolymers, core-shell micellar structures with a dense PLA core and a hydrated PMeOx shell in the whole range of *f* values. The triblock copolymers formed micellar aggregates of finite sizes made of bridged micelles, the micelles being connected by some of the PLA end-blocks. Moreover, the micelles displayed original core-multishell nanostructures in a specific

range of *f* values (48 %), never reported for this kind of triblock copolymers. The amphiphilic copolymers of this study displayed a rich variety of controlled self-assembled morphologies which could be promising candidates for drug delivery applications.

Introduction

Amphiphilic block copolymers capable of self-assembling into micellar structures drain a large interest over the last decades to improve hydrophobic drug encapsulation and delivery because of the mesoscopic size range and the high drug-loading capacity of the inner core.[1-4] In this aim, several ABA poloxamer poly(ethylene glycol)-*b*-poly(propylene oxide)-*b*-poly(ethylene glycol) (PEG-*b*-PPO-*b*-PEG), commercially available under the name pluronic received attention because of their self-assembly in core-shell micelles capable of passing physiological barriers such as the blood-brain barrier.[5,6] The PPO block ensures the hydrophobic cohesion and subsequently the encapsulation of hydrophobic active compounds while the PEG block is the shell-stabilizing segment. Due to its high water solubility, remarkable stealth properties and apparent low toxicity, many efforts have been carried out to elaborate a large library of amphiphilic copolymers based on PEG. In this way, Kataoka and co-workers[7,8] performed a one-pot synthesis of α-acetal-poly(ethylene glycol)-*b*-poly(D,L-lactide) (α-acetal-PEG-PLA). Then, the dialysis against water was employed to prepare polymeric micelles of 31 nm, after the solubilization of block copolymer in dimethylacetamide (DMAc), a good solvent for both segments. More recently, amphiphilic copolymers based on PEG and poly(amino acid) block able to form nanometric structures showed a large interest for drug and gene delivery,[9] in part because polypeptide conformation can influence their aggregation behavior in aqueous medium.[10,11]

However, several studies revealed important drawbacks of PEG. Due to the intensive use of PEG, PEGylated systems have lost their stealth function when applied *in vivo*, because of the existence of non-specific and specific recognition by the immune system. Indeed, specific antibodies were detected in the serum of patients treated with PEG-asparaginase[12] and PEG-uricase.[13] In addition, PEG-specific antibodies were identified in 25 % of patients who had never received treatment based on PEG, due to the presence of PEG in many food and cosmetic products.[14,15] These antibodies have a neutralizing effect and cause a significant loss of the expected therapeutic effect.

To solve this problem, different polymer families are considered as possible alternatives to PEG for biomedical uses: poly(vinylpyrrolidone) (PVP), poly(*N*-(2-hydroxypropyl) methacrylamide) (PHPMA), synthetic hydrophilic polypeptides and poly(oxazoline)s.[16] Particularly poly(2-methyl-2-oxazoline) (PMeOx) and poly(2-ethyl-2-oxazoline) (PEtOx) are often compared to PEG because they present similar chain flexibility in physiological media,[17] same stealth behavior towards plasmatic protein [18-20] and a better biocompatibility.[21,22] Amphiphilic diblock and triblock copolymers based on PMeOx have been reported in the literature.[23-27] In these works, hydrophobic blocks were of different natures, going from fluid blocks made of low glass transition temperature (T_g) polymers such as polydimethylsiloxane,[23] poly(tetrahydrofuran)[24] or poly(2-(1-ethylheptyl)-1,3-oxazoline)[25] or poly(2-nonyl-2-oxazoline)[26] to frozen blocks made of high T_g polymers such as poly(2-phenyl-2-oxazoline).[27]

Despite the well-known interesting and often reported properties of poly(lactide) (PLA), such as biocompatibility and biodegradability,[28,29] and extensive description within PEG/PLA-based systems both in term of synthesis strategies, biofunctionalization, colloidal stability, physico-chemical characterization and drug encapsulation,[7,8,30-33] only a few works were

related to self-assembly study of amphiphilic block copolymer combining poly(2-oxazoline) with PLA, which behave as frozen block at ambient temperature.[34]

Moreover, the control of the characteristics of polymeric micelles, such as size, shape and surface properties characterization, have crucial importance, to optimize drug encapsulation and then delivery as well as to maintain colloidal staibilty.[35,36] In addition, the distribution of drug-loaded polymeric micelles in the body may be determined mainly by their size and morphology and is less affected by the properties of loaded drugs if these are embedded in the inner core of the micelles. Indeed, a nanometric size range from 10 to 200 nm is a crucial factor in determining their body disposition, especially when an enhanced permeation retention effect (EPR effect) is involved.[37-40] Consequently, a thorough characterization of their size and structure at nanometer resolution is a prerequisite.

In this context, we propose the elaboration of amphiphilic diblock and triblock copolymers poly(2-methyl-2-oxazoline)-*b*-poly(D,L lactide) (PMeOx-*b*-PLA) and poly(D,L lactide)-*b*-poly(2-methyl-2-oxazoline)-*b*-poly(D,L lactide) ((PLA-*b*-PMeOx-*b*-PLA) and their self-assembly in water. It should be emphasized that contrary to the literature works where the middle block was hydrophobic, the hydrophilic block was set in the middle of the triblock copolymers synthesized, leading to another variety of supramolecular structures. Two processes were used, the nanoprecipitation and the dialysis to rationalize the relationship between copolymer structure, method of self-assembly and the morphology of the micelles by using dynamic light scattering (DLS), small angle neutron scattering (SANS) and cryo-TEM.

Materials and methods

Materials

The high-molecular-mass poly(D,L-lactide) (PLA) was purchased from Cargill Laboratories (Cedar Grove, NJ, USA). The monomer 2-methyl-2-oxazoline (Sigma-Aldrich, Saint-Louis, MO, USA, purity 99 %) were dried overnight over calcium hydride and purified by distillation under an argon atmosphere. Sodium azide (NaN_3) (BioUltra, purity ≥ 99.5 %), anhydrous acetonitrile (ACN) (purity 99,8%), 1-iodobutane (purity 99%), 1,3-diiodopropane (purity 99%) were purchased from Sigma Aldrich and used as received. Dimethylsulfoxide (DMSO), diethyl ether and dichloromethane were purchased from Carlo Erba (Val de Reuil, France) and used without extra purification. *N,N*-Dimethylformamide (DMF) was purchased from VWR (Radnor, Pennsylvania, USA). Copper commercially available nanopowder (Cu NPs) with nominal size from 20 nm to 40 nm was purchased from Alfa Aesar (Haverhill, MA, USA).

Polymers synthesis

Synthesis of functionalized polymers: alkynyl-terminated poly(D,L-lactide) and azide-terminated poly(2-methyl-2-oxazoline)

Alkynyl-terminated poly(D,L-lactide) (PLA≡) oligomers were prepared *via* transesterification of high-molecular-mass PLA ($\overline{M_n}$= 8.72×10^4 g.mol^{-1}, $Đ = \frac{\overline{M_w}}{\overline{M_n}} = 2$) as previously reported.[41]

^{1}H NMR (400 MHz, $CDCl_3$): δ = 5.14 (q, 1H, C*H*(CH_3), 4.69 (m, 2H, C*H*$_2$CCH), 4.31 (m, 1H, HOC*H*CH_3), 2.66 (s, 1H, OH), 2.48 (t, 1H, *H*CC), 1.56 (d, 3H, CH_3) ppm.

FTIR (ATR mode): C-H 2996, 2946 cm^{-1}; C≡C 2124 cm^{-1}; C=O 1754 cm^{-1}; C-O 1180 cm^{-1}.

α-Azide-terminated poly(2-methyl-2-oxazoline) (PMeOx-N_3) and α-, ω-azide-functionalized poly(2-methyl-2-oxazoline) (N_3-PMeOx-N_3) were synthesized *via* cationic ring-opening

polymerization (CROP). Various [monomer]/[initiator] molar ratios were used to obtain polymers with different molecular masses. For PMeOx-N_3, as an example, a solution of 2-methyl-2-oxazoline (4.0 mL, 47.2 mmol) and 1-iodobutane as initiator (230 µL, 2.01 mmol) in dry acetonitrile (ACN) (12.0 mL) was stirred at 80 °C, under dry argon. After 5 hours, the necessary time for total monomer consumption, determined by the kinetic study previously conducted,[42] polymer was functionalized by adding an excess of NaN_3, and the reaction mixture was stirred for 24 hours still at 80 °C. The polymer obtained was purified by precipitation in diethyl ether, filtered and dried under vacuum at 60 °C to afford a white powder (yield = 95 %). Two polymers were synthesized with different number-average molecular masses $\overline{M_n}$: 2.2×10^3 and 5.5×10^3 g.mol^{-1}. A similar procedure was used to synthesize telechelic polymers N_3-PMeOx-N_3 using a bifunctional initiator, the 1,3-diiodopropane and knowing the polymerization constant.[43] The telechelic polymers obtained had $\overline{M_n}$ of 2.2×10^3 and 8.2×10^3 g.mol^{-1}.

Synthesis of amphiphilic copolymers: PMeOx-b-PLA and PLA-b-PMeOx-b-PLA

The amphiphilic diblock and triblock copolymers, poly[(2-methyl-2-oxazoline)-*b*-poly(D,L-lactide)] (PMeOx-*b*-PLA) and poly[(D,L-lactide)-*b*-(2-methyl-2-oxazoline)-*b*-(D,L-lactide)] (PLA-*b*-PMeOx-*b*-PLA), were obtained by coupling the alkynyl-PLA with the azide end group of the functionalized PMeOx-N_3 or N_3-PMeOx-N_3. Typically, to obtain the diblock copolymer ($PMeOx_{2200}$-*b*-PLA_{2800}), PLA≡ (2.8×10^3 g.mol^{-1}, 100 mg, 3.57×10^{-2} mmol) and 1.1 equivalent of PMeOx-N_3 (2.2×10^3 g.mol^{-1}, 87.0 mg, 3.95×10^{-2} mmol), were dissolved in 10 mL of dry DMSO and 10 mg of commercially available copper nanoparticles (Cu NPs) were added. The reaction mixture was then subjected to microwave irradiation under stirring at 80 °C for 25 min. Cu NPs were removed by centrifugation at 4000 rpm for 10 min. The supernatant was centrifuged a second time and purified by dialysis against water (molecular

weight cut off: 3.5 KDa or 6-8 KDa depending on the PMeOx molecular mass). The diblock copolymer was recovered by freeze-drying (yield = 79 - 85 %). The amphiphilic triblock copolymers PLA-*b*-PMeOx-*b*-PLA were obtained from a similar procedure using the telechelic polymers N_3-PMeOx-N_3 (yield = 73 - 92 %).

Nanoprecipitation and dialysis methods

Self-assembly of diblock copolymers were prepared using the nanoprecipitation method: 1 ml of solution of copolymer in acetonitrile (ACN) with a concentration of 2 $g.L^{-1}$ was stirred and added dropwise in 2 mL of ultrapure water at 25 °C stirred at 220 rpm. The organic solvent was removed from the dispersion by evaporation under reduced pressure at room temperature and the volume was adjusted by addition of ultrapure water to obtain a concentration of 1 $g.L^{-1}$.

Self-assembly of triblock copolymers were prepared with the same nanoprecipitation procedure and by the dialysis method. Concretely, a solution of copolymer in ACN at a concentration of 1 $g.L^{-1}$ was dialyzed against water for 2 days (Spectra/Por dialysis tubing, molecular weight cut off 6-8000 Da). The volume of water was 500 mL and was renewed 5 times per day. Finally, the volume of the suspension was adjusted by evaporation under vacuum to obtain a concentration of 1 $g.L^{-1}$.

Instrumentation and Measurements

Fourier-transform infrared spectroscopy (FTIR) spectra were recorded on a Bruker Tensor 27 instrument equipped with a Digi Tect DLaTGS detector, 32 scans were collected at a resolution of 1 cm^{-1} using an ATR accessory (single-reflection horizontal ATR, Miracle, Pike

Technologies). Chemical structures of the polymers were investigated using a Raman apparatus Xplora from Horiba Jobin Yvon (Longjumeau, France) equipped with a laser emitting at 638 nm. The acquisition time was fixed at 1 min. ^{1}H nuclear magnetic resonance spectroscopy (NMR) experiments were performed in D_2O, $CDCl_3$ or DMSO-d_6 at 25 °C on a Bruker NMR spectrometer operating at 400 MHz equipped with a Bruker multinuclear z-gradient direct probe head capable of producing gradients in the z direction with 53.5 G.cm^{-1} strength. ^{1}H NMR spectra were recorded with 64 scans and a relaxation time of 4 sec. Size exclusion chromatography (SEC) of polymers was performed in two different solvents: aqueous eluent (0.1 mol.L^{-1} $LiNO_3$) for the azide-terminated poly(2-methyl-2-oxazoline) and *N,N*-Dimethylformamide (DMF) for the other polymers. In the case of aqueous eluent (0.1 mol.L^{-1} $LiNO_3$), the chromatograph is equipped with a pump P 100 (Spectra-Physics, Fremont, CA, USA) and a 1260 Infinity automatic injector (Agilent Technologies, Santa Clara, CA, USA). For the analysis of polymers in aqueous eluent (0.1 mol.L^{-1} $LiNO_3$), a set of two columns PL-aquagel OH-30 and OH-40 (Polymer Laboratories, Shropshire, UK) was used. Two detectors were connected in series at the end of the columns: a Dawn Optilab Rex differential refractometer and a Dawn Heleos 8 light scattering detector (Wyatt Technology, Santa Barbara, CA, USA). In the case of DMF eluent, SEC was performed on a Waters equipment with refractive index detector and a Shodex KD-806M column that was calibrated with poly(ethylene oxide) standards. The chromatographic analysis of polymers was done with all polymer solutions at a concentration of 10 mg mL^{-1}.

Thermogravimetric analyses (TGA) were performed on a Setaram Setsys Evolution 16 apparatus by heating the samples at a rate of 10 °C.min^{-1} from 20 °C to 800 °C under argon atmosphere.

To determine the hydrodynamic radius (R_h) and the polydispersity index (PDI, a dimensionless measure of the broadness of the size distribution), dynamic light scattering

(DLS) measurements were performed on a Malvern Instruments Zetasizer Nano ZS operating with a He-Ne laser source at the wavelength of 633 nm. All measurements were performed at 25 °C and at a scattering angle of 173°. The concentration of the solutions was 1 $mg.mL^{-1}$. The autocorrelation functions ($g_1(t)$) were analyzed in terms of relaxation time distribution (τ) (equation 1).

$$g_1(t) = \int A_{(\tau)} \exp\left(\frac{-t}{\tau}\right) d\tau \quad (1)$$

Hydrodynamic radius (R_h) was determined from the Stokes-Einstein relation (equation 2).

$$R_h = \frac{k_B T}{6\pi\eta_s D_0} \quad (2)$$

Where D_0 is diffusion coefficient, η_s ids the viscosity of the solvent, T is absolute temperature and k_B the Boltzmann constant. The correlation functions were also analyzed using the cumulants method to derive the mean radii and polydispersity index (PDI) of the nanoparticles. In case of PDI lower than 0.3, the distribution width, σ_{DLS}, can be approximated as $(PDI)^{1/2}$.

For the cryo-transmission electron microscopy (Cryo-TEM), a drop of NPs suspension was deposited on "quantifoil"® (Quantifoil Micro Tools GmbH, Germany) carbon membrane. The excess of liquid on the membrane was blotted out with a filter paper and, before evaporation, the membrane was quench-frozen in liquid ethane to form a thin vitreous ice film in which NPs were captive. Once mounted in a Gatan 626 cryo-holder cooled with liquid nitrogen, the samples were transferred in the microscope and observed at low temperature (-180 °C). Cryo-TEM images were recorded on an ultrascan 2k ccd camera (Gatan, USA), using a LaB6 JEOL 2100 (JEOL, Japan) cryo-microscope operating at 200kV with a JEOL low dose system (Minimum Dose System, MDS) to protect the thin ice film from any irradiation before imaging and reduce the irradiation during the image capture.

Small-angle neutron scattering (SANS) measurements were performed at the Laboratoire Léon Brillouin ("ORPHEE" reactor, CEA Saclay) on the "PACE" spectrometer. The experimental scattering vector q ($q = (4\pi / \lambda) \sin(\theta/2)$) range was $0.0032 < q$ (Å^{-1}) < 0.44 and was covered by three sample-to-detector distances and two different wavelengths (1 or 3 m at the neutron wavelength of 5 Å and 4.5 m at 13 Å). The samples were loaded into Hellma quartz cells with a 2 mm optical path length. The cells were placed in a sample changer, and the scattering for each sample was measured for about 1.5 hour at room temperature. Scattering intensities from solutions were corrected for empty cell scattering and sample transmission. $I(q)$ is in absolute scale (cm^{-1}). For all samples, the solvent scattering intensity was subtracted, but we have not succeeded in completely removing the sample background (which is inferior to 1×10^{-3} cm^{-1}). All colloidal suspensions were prepared as previously explained and then dialyzed against D_2O, and the concentration was 1 g.L^{-1} unless specified.

Fits: 2 types of model fitting provided by SasView software (http://www.sasview.org) were used. Polydisperse sphere model describes a sphere with a lognormal distribution on the radius r_s (Equation 3).

$$I(q,r) = \frac{I_0}{V}\left[3V(\rho_s - \rho_{solv})P_{sp}(q,r)\right]^2 \qquad (3)$$

Where $P_{sp}(q,r)$ is the form factor for a monodisperse spherical particle with uniform scattering length density ρ_s, ρ_s value has been fixed as the scattering length density of PLA.

Polydisperse core-multishell model (Equation 4) consists in a core of radius r_c, spherical shells with thicknesses δ_1 ($\delta_1 = r_{s1} - r_c$) and δ_2 ($\delta_2 = r_{s2} - r_{s1}$), r_{s1} and r_{s1} being respectively the radius of the first and the second shell. We applied a lognormal distribution for r_c, r_{s1} and r_{s2}.

$$I\left(q, r_{c,} r_{s1}, r_{s2,}\right) = \frac{I_0}{V_s}\Big[3V_c(\rho_c - \rho_{s1})P_{sp}(q,r_c) + 3V_{s1}(\rho_{s1} - \rho_{s2})\big[V_{s1}P_{sp}(q,r_{s1}) -$$

$$V_cP_{sp}(q,r_c)\big] + 3V_{s2}(\rho_{s2} - \rho_{solv})\big[V_{s2}P_{sp}(q,r_{s2}) - V_{s1}P_{sp}(q,r_{s1})\big]\Big]^2 \qquad (4)$$

Where $P_{sp}(q,r)$ has been previously defined. ρ_c, ρ_{s1}, ρ_{s2}, ρ_{sol} are respectively the neutron scattering length density of the core, the shell 1, the shell 2 and the solvent.

Results and discussion

Synthesis and characterization of di- and triblock copolymers.

First, the functionalized polymers were prepared by cationic ring opening polymerization (CROP) for poly(2-methyl-2-oxazoline) (PMeOx) and by transesterification for poly(D,L-lactide) (PLA). In a second step, the block copolymers were built by "click" chemistry. The CROP of 2-methyl-2-oxazoline was performed, as described previously,[27, 25] in anhydrous ACN at 80 °C, using 1-iodobutane or 1,3-diiodopropane as initiator and NaN_3 as termination agent to obtain α-azide-terminated poly(2-methyl-2-oxazoline) (PMeOx-N_3) and α-, ω-azide-functionalized poly(2-methyl-2-oxazoline) (N_3-PMeOx-N_3) respectively. The polymers were fully characterized by ^{1}H NMR and SEC. The ^{1}H NMR spectra of the PMeOx-N_3 and N_3-PMeOx-N_3 (Figure S1 and S2) were performed in D_2O and $CDCl_3$ respectively. The degrees of polymerization and consequently the number-average molecular masses ($\overline{M_n}^{NMR}$) of the polymers were calculated using the integration of the peaks **1** at 2.08 ppm, corresponding to the repetitive unit and the integration of the peak **a** at 0.92 ppm corresponding to the protons of methyl end group in the case of PMeOx-N_3 or the integration of the peaks **a** at 1.18 ppm corresponding to the methylene protons of the bifunctional initiator in the case of N_3-PMeOx-N_3. The polymers obtained were characterized by SEC in aqueous solution with LS detector to obtain absolute number-average molecular masses $\overline{M_n}^{SEC}$ reported in Table S1. A good agreement was observed between the $\overline{M_n}^{NMR}$, $\overline{M_n}^{SEC}$ and the expected molecular masses

calculated from the feed ratio $\overline{M_n}^{expected}$. Chromatograms highlighted monomodal distributions (Figure S3) with narrow dispersities indicating the controlled character of the polymerizations. The presence of the azide end groups, for all polymers, was confirmed by FTIR with the band at 2097 cm^{-1} (Figure S4). Alkynyl-terminated PLA (PLA≡) was previously prepared by direct transesterification reaction as reported elsewhere.[25] This method has the major advantage to produce oligomers with an alkynyl end group in a one-step reaction. The average-number molecular mass and the chemical structure of the alkynyl-terminated PLA were previously confirmed by SEC, ^{1}H NMR and Raman spectroscopy.[44] A series of five oligomers were prepared with number-average molecular masses ranging from 1.2×10^3 to 5.2×10^3 $g.mol^{-1}$ with dispersity values from 1.3 to 1.5.

The di- and triblock copolymers were prepared using the copper-catalyzed Huisgen [3+2] cycloaddition "click" chemistry between azide and alkyne (CuAAC) (Scheme 1). The "click" reaction was catalyzed by copper nanoparticles (Cu NPs) in dimethylsulfoxide (DMSO) at 80 °C. The $[N_3]/[C\equiv C]$ feed ratio was maintained at 1.1, and the reaction was conducted for 25 min under microwave irradiation. The purification of the block copolymers was simplified using copper nanoparticles as the Cu NPs could be easily removed by centrifugation.

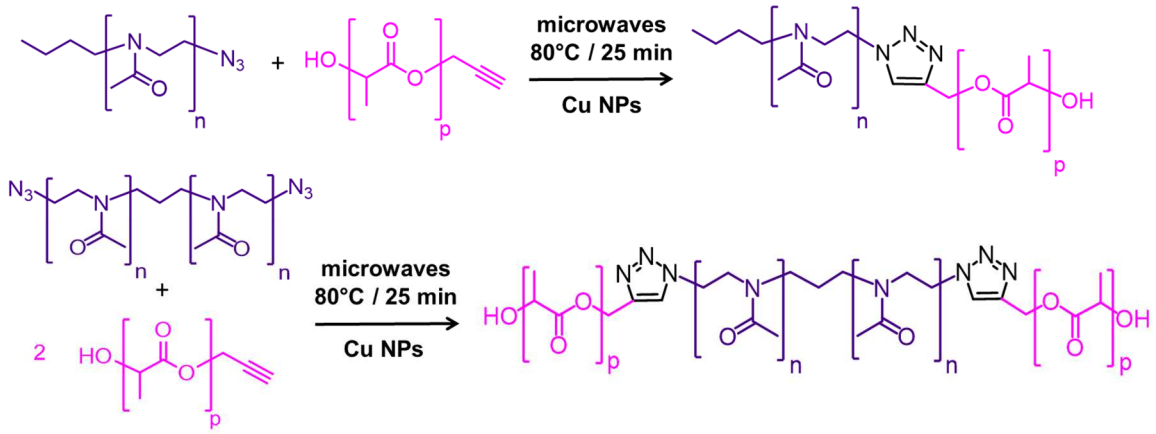

Scheme 1. Synthesis of PMeOx *b*-PLA and PLA-*b*-PMeOx *b*-PLA by Huisgen 1,3-dipolar cycloaddition with copper-nanoparticles (Cu NPs) as catalyst.

The copolymers were characterized by SEC in DMF using a poly(ethylene oxide) (PEO) calibration curve. The chromatograms have shown monomodal distributions, as reported in Figure S5 for a diblock and a triblock copolymer. This is a first indication of the coupling efficiency between the different blocks. The quantitative results are reported in Table S2. For comparison, the homopolymers PLA≡ , PMeOx-N_3 and N_3-PMeOx-N_3 were also analyzed in DMF. For PLA≡ , there is a good agreement between the $\overline{M_n}^{SEC}$ and $\overline{M_n}^{expected}$ but the molecular weights determined for PMeOx are lower than the expected values and are also lower than the molecular weights determined by light scattering detector in aqueous eluent (Table S1). This discrepancy could be attributed to a more compact conformation of PMeOX chains than PEO standards. The molecular weights determined for the copolymers indicated also a similar discrepancy between the molecular weights determined from the PEO calibration curve and $\overline{M_n}^{expected}$ and this can be attributed to the more compact conformations of the copolymers in DMF than PEO chains. Nevertheless, the molecular weights increased, as expected, with the molar masses of each block.

The efficiency of the coupling reaction between the azido and alkynyl end groups was then demonstrated by FTIR and Raman spectroscopy, two perfectly complementary techniques. The success of the cycloaddition reaction, for the diblock and triblock copolymers, was confirmed by FTIR with the total disappearance of the azide signal at 2097 cm^{-1} (Figure 1A) and by Raman spectroscopy (Figure 1B) with the disappearance of the signal corresponding to the alkyne end function of the PLA at 2131 cm^{-1}.

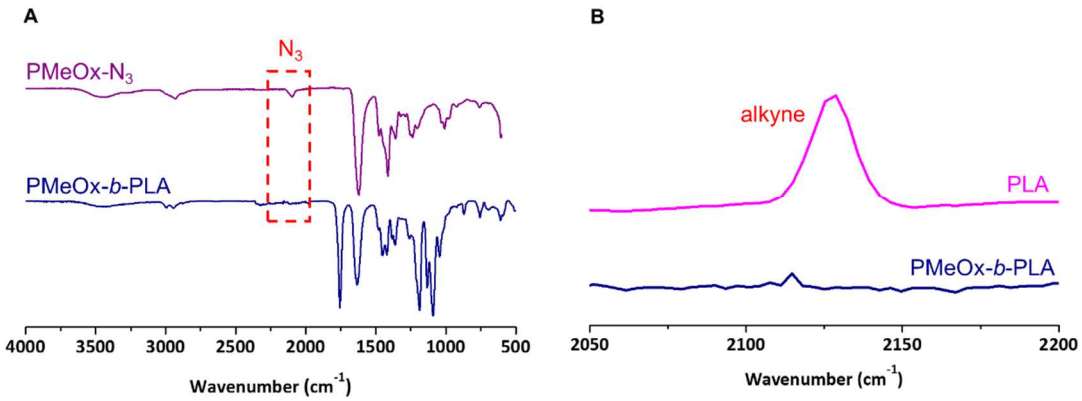

Figure 1. (A) FTIR of spectra of PMeOx$_{2200}$-N$_3$ and PMeOx$_{2200}$-*b*-PLA$_{2800}$ and (B) RAMAN spectra of PLA≡ and PMeOx$_{2200}$-*b*-PLA$_{2800}$

The chemical structure of diblock copolymers PMeOx-*b*-PLA was investigated by ^{1}H NMR in DMSO-d$_6$ (Figure 2). Coupling was attested by the appearance of the peak of resonance **t** at 8.20 ppm corresponding to the triazole proton **t** resulting from the CuAAC, and by the expected downfield shift of the peak **4** observed for the methylene protons in α of triazole compared to the one in α of the azide group (from 3.32 to 4.55 ppm). Furthermore, in the DMSO-d$_6$, the protons of this signal **4**, are not equivalent due to the lack of mobility in α of the triazole ring, so the signal observed is a doublet. Finally, the total shift of the peak **5** corresponding to the proton on the carbon of the PLA in α of the triazole ring (from 4.85 in PLA≡ to 5.20 ppm in coupled PLA) confirmed the success of the click reaction.

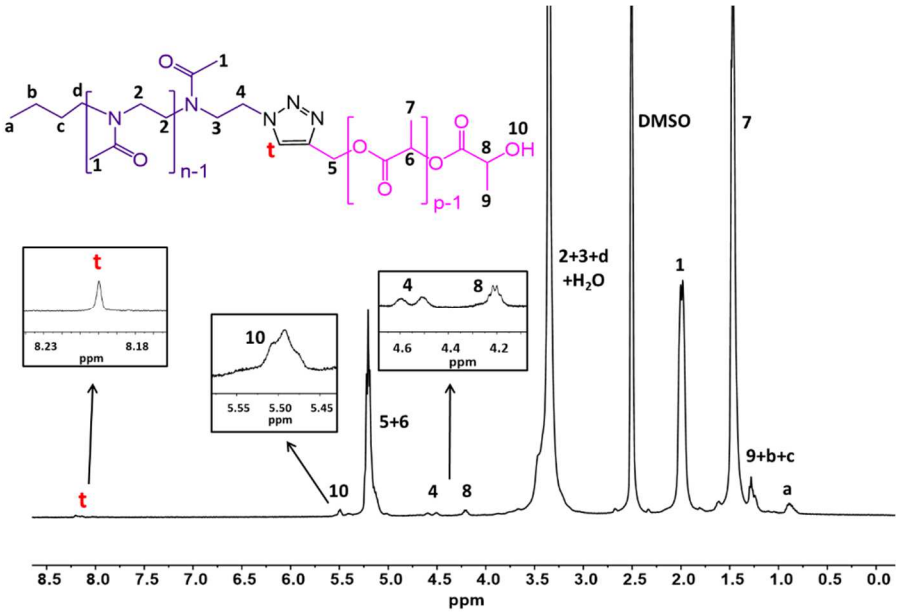

Figure 2. ^{1}H NMR spectrum of a diblock copolymer PMeOx$_{2200}$-*b*-PLA$_{2800}$ in DMSO-d$_6$

The ^{1}H NMR spectra of the triblock copolymers PLA-*b*-PMeOx-*b*-PLA were performed in $CDCl_3$ (Figure 3). The presence of the peak of resonance **t** at 7.59 ppm corresponding to the proton of the triazole rings as well as the downfield shift of the peak**s 4** at 4.55 ppm and **3** at 3.80 ppm in α and β of the triazole with respect to the signal in α and β of azide group showed the coupling.

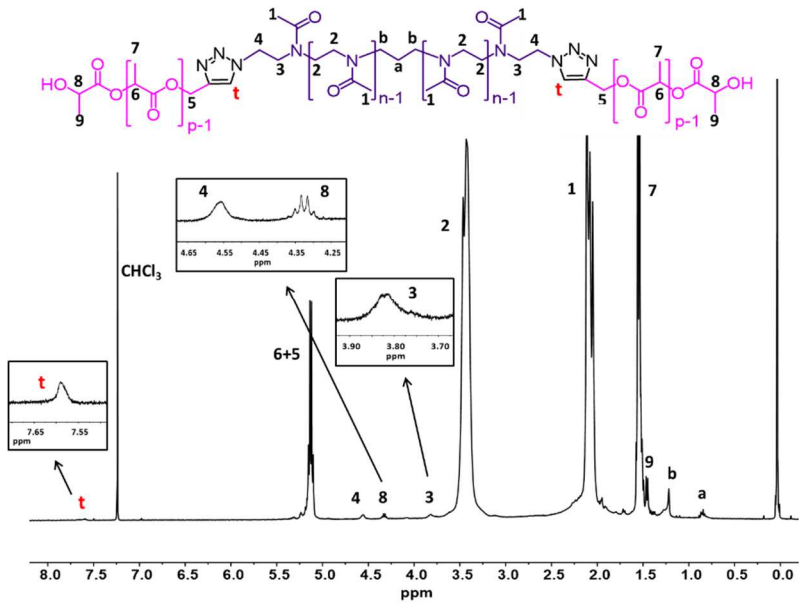

Figure 3. ^{1}H NMR spectrum of a triblock copolymer PLA$_{2200}$-*b*-PMeOx$_{2200}$-*b*-PLA$_{2200}$ in $CDCl_3$.

It is interesting to note that the signal **4**, for the diblock as for the triblock copolymers, is a singlet in the $CDCl_3$ and a doublet in DMSO-d_6. Finally, the total shift of the signal **5** corresponding to the proton on the carbon of the PLA in α of the triazole ring (from 4.70 to 5.10 ppm) and, in COSY NMR (Figure S6), the absence of correlation signal corresponding to the methylene proton adjacent to terminal alkyne group before the cycloaddition confirmed the success of the click reaction and the absence of free alkynyl-terminated PLA. The characterization of the four synthesized diblock copolymers and of the six triblock copolymers including number-average molecular masses of each block and the fraction of the molecular mass of the hydrophilic part to the total molecular mass (*f*) are summarized in Tables 1 and 2.

Table 1. Diblock copolymers PMeOx-*b*-PLA: molecular characteristics and weight fractions of PLA.

Copolymers	$\overline{M_n}^{PMeOx}$ (g.mol^{-1})	$\overline{M_n}^{PLA}$ (g.mol^{-1})	$\overline{M_n}^{diblock}_{calculated}$ (g.mol^{-1})	PLA wt. % expected	PLA wt. % NMR	PLA wt. % TGA	*f* (%)
PMeOx$_{2200}$-*b*-PLA$_{2800}$	2.2×10^3	2.8×10^3	5.0×10^3	56	58	57	44
PMeOx$_{2200}$-*b*-PLA$_{5200}$	2.2×10^3	5.2×10^3	7.4×10^3	70	75	76	30
PMeOx$_{5500}$-*b*-PLA$_{2800}$	5.5×10^3	2.8×10^3	8.3×10^3	34	34	32	66
PMeOx$_{5500}$-*b*-PLA$_{5200}$	5.5×10^3	5.2×10^3	10.7×10^3	48	52	50	52

f: hydrophilic weight ratio (ratio of the mass of the hydrophilic part to the total mass)

Table 2. Triblock copolymers PLA-*b*-PMeOx-*b*-PLA: molecular characteristics and weight fractions of PLA.

Copolymers	$\overline{M_n}^{PMeOx}$ (g.mol^{-1})	$\overline{M_n}^{PLA}$ (g.mol^{-1})	$\overline{M_n}^{triblock}_{calculated}$ (g.mol^{-1})	PLA wt. % expected	PLA wt. % NMR	PLA wt. % TGA	*f* (%)
PLA_{1200}-*b*-$PMeOx_{2200}$-*b*-PLA_{1200}	2.2×10^3	1.2×10^3	4.6×10^3	52	55	54	48
PLA_{2200}-*b*-$PMeOx_{2200}$-*b*-PLA_{2200}	2.2×10^3	2.2×10^3	6.6×10^3	66	69	65	34
PLA_{4200}-*b*-$PMeOx_{2200}$-*b*-PLA_{4200}	2.2×10^3	4.2×10^3	10.6×10^3	79	81	78	21
PLA_{1200}-*b*-$PMeOx_{8200}$-*b*-PLA_{1200}	8.2×10^3	1.2×10^3	10.6×10^3	23	25	25	77
PLA_{2200}-*b*-$PMeOx_{8200}$-*b*-PLA_{2200}	8.2×10^3	2.2×10^3	12.6×10^3	34	35	30	67
PLA_{4200}-*b*-$PMeOx_{8200}$-*b*-PLA_{4200}	8.2×10^3	4.2×10^3	16.6×10^3	50	52	48	50

f: hydrophilic weight ratio (ratio of the mass of the hydrophilic part to the total mass)

Thermal stability of the diblock and triblock copolymers was studied by thermogravimetric analyses (TGA) (Figure 4) and compared with the degradation profiles of the PMeOx-N_3 or N_3-PMeOx-N_3 and the PLA≡.

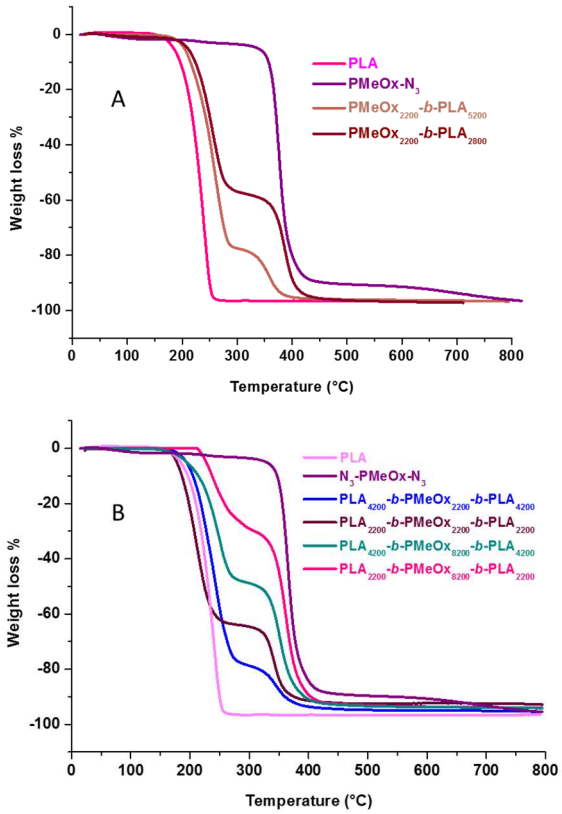

Figure 4. TGA curves for PLA≡, PMeOx-N_3 and PMeOx *b*-PLA (A) and for PLA≡ and N_3-PMeOx-N_3 and PLA-*b*-PMeOx *b*-PLA (B).

The obtained results showed a two-step degradation behavior with a first step from 200 to 280 °C (or 150 to 250 °C) corresponding to the degradation of the PLA block and a second step from 280 to 440 °C (or 250 to 450 °C) corresponding to the degradation of PMeOx block. The weight fraction of PLA in each copolymer was calculated and the results (summarized in Tables 1 and 2) demonstrated a good correlation with those obtained by ^{1}H NMR and with the expected values. Thereby, these results confirmed the efficiency of the coupling reaction for the preparation of amphiphilic diblock and triblock copolymers PMeOx-*b*-PLA and PLA-*b*-PMeOx-*b*-PLA with various hydrophilic weight ratios (*f*).

Self-assembly study of the diblock copolymers

Self-assemblies of the diblock copolymers were prepared by nanoprecipitation, that is commonly known for resulting in kinetically trapped structures due to rapid solvent exchange.[45] First, the PMeOx-*b*-PLA diblock copolymers were dissolved in acetonitrile (ACN) (2 g L^{-1}), which is a solvent for both PMeOx and PLA polymers and has a good miscibility with water. The solution was added dropwise to deionized water, under moderate stirring, inducing the self-assembly process. The organic solvent was then removed under vacuum and water added to reach the desired concentration. Herein, the different diblock copolymers used were, in increasing order of hydrophilic weight ratio *f*: $PMeOx_{2200}$-*b*-PLA_{5200} (*f* = 30 %), $PMeOx_{2200}$-*b*-PLA_{2800} (*f* = 44 %), $PMeOx_{5500}$-*b*-PLA_{5200} (*f* = 52 %) and $PMeOx_{5500}$-*b*-PLA_{2800} (*f* = 66 %).

The resulting suspensions were characterized by dynamic light scattering (DLS) at 173°, the results showed the presence of nano-objects with hydrodynamic radius (R_h) between 14 nm and 24 nm according to the composition of the amphiphilic copolymer, as well as objects of several hundred nanometers (as shown in the Figure 5.A for the distribution based on $PMeOx_{2200}$-*b*-PLA_{2800}). The distribution widths (σ_{DLS}) are high, of the order of 0.5, because of the bimodal size distribution (only in intensity, volume size distributions showed a unimodal distribution). The R_h (from volume size distribution) and σ_{DLS} values are reported in Table 3.

The cryo-TEM micrographs of the suspension based on $PMeOx_{2200}$-*b*-PLA_{2800} (Figure 5.B) allowed observing spherical objects with an average radius of 15 nm (average radius was calculated on the basis of at least 100 nano-objects using imageJ software) which is extremely close to the R_h obtained by DLS. It should be noted the absence of large aggregates, around about 200 nm, in cryo-TEM, suggesting that they are few, which is

consistent with their presence in DLS only in intensity, not in volume.

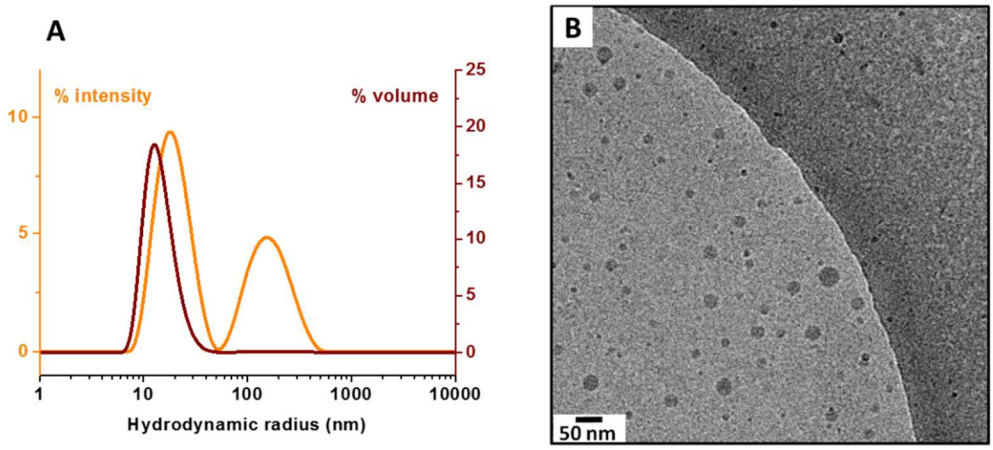

Figure 5. (A) DLS size distribution and (B) cryo-TEM micrograph of nano-objects of $PMeOx_{2200}$-*b*-PLA_{2800} (f = 44 %) obtained by nanoprecipitation.

Small-angle neutron scattering (SANS) was used to probe more precisely and quantitatively the structure of the nano-objects and to measure better averaged nanoscopic dimensions of the objects through an appropriate model. As said before, the suspensions were analyzed in D_2O at a concentration of 1 $g.L^{-1}$ at room temperature. Figure 6 shows the scattered intensity as a function of scattering vector (q) for nano-objects based on $PMeOx_{2200}$-*b*-PLA_{5200} (f = 30%) (pink circle), $PMeOx_{2200}$-*b*-PLA_{2800} (f = 44%) (red square) and $PMeOx_{5500}$-*b*-PLA_{52000} (f = 52 %) (orange triangle) (for better visibility, scattered intensities of red and orange curves were multiplied by a power of 10 on the graph).

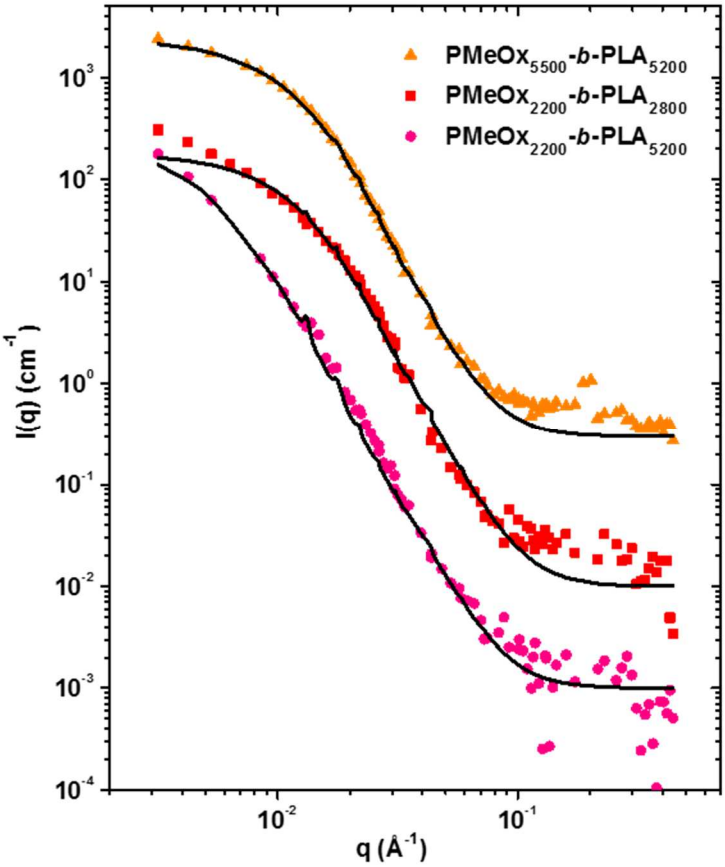

Figure 6. Scattered intensity as a function of scattering vector for nano-objects of PMeOx$_{2200}$-*b*-PLA$_{5200}$ (f = 30 %), PMeOx$_{2200}$-*b*-PLA$_{2800}$ (f = 44 %), and PMeOx$_{5500}$-*b*-PLA$_{5200}$ (f = 52 %) (the black line is the fitting curve by a polydisperse sphere model).

The general appearance of the three curves was similar for large and medium q values. Indeed, the intermediate q value regime (2.0×10^{-2} < q (Å^{-1}) < 8.0×10^{-2}) is characterized by a variation in q^{-4} and might correspond to a compact structure. While for larger values of q (8.0×10^{-2} < q (Å^{-1}) < 4.4×10^{-1}), the decrease of log I was less abrupt. This variation might be characteristic of an interface of dangling polymer chains. However, the absence of a variation in q^{-2} was due to the impossibility to subtract more incoherent from the solvent. Nevertheless, for small values of scattering vector q, it is possible to observe, for samples based on PMeOx$_{2200}$-*b*-PLA$_{2800}$ and PMeOx$_{5500}$-*b*-PLA$_{5200}$, a plateau (Guinier regime) characteristic of

a size approachable by SANS, while for samples based on PMeOx$_{2200}$-*b*-PLA$_{5200}$ this plateau was not reached which might correspond to a greater polydispersity and / or larger radius of gyration.

The SANS data were fitted using a polydisperse sphere model. The dispersities due to the detector, on the I and q values, have been considered. The traces of the fits obtained are in black on the Figure 6. The parameters of the fits (R_{SANS} and σ_{SANS}) are reported in Table 3.

Table 3. Characteristics of PMeOx-*b*-PLA self-assemblies obtained by nanoprecipitation.

Copolymers	*f* (%)	R_h [(a)] (nm)	σ_{DLS}[(a)]	R_{SANS}[(b)] (nm)	σ_{SANS} [(b)]	Lc(PMeOx) (nm)	Lc(PLA) (nm)	N_{agg} [(c)]
PMeOx$_{2200}$-*b*-PLA$_{5200}$	30	23.5	0.59	16.7	0.44	9.0	26.0	2800
PMeOx$_{2200}$-*b*-PLA$_{2800}$	44	14.5	0.67	9.9	0.40	9.0	14.0	1090
PMeOx$_{5500}$-*b*-PLA$_{5200}$	52	24.5	0.47	9.5	0.37	22.6	26.0	520
PMeOx$_{5500}$-*b*-PLA$_{2800}$	66	22.0	0.55	-	-	22.6	14.0	-

(a) Hydrodynamic radii and σ_{DLS} values determined by DLS

(b) Determined by fitting the SANS curves using a polydisperse sphere model.

(c) Aggregation number.

One can notice that R_{SANS} were always lower than R_h for all the samples analyzed by the two methods. For instance, for PMeOx$_{2200}$-*b*-PLA$_{2800}$, R_{SANS} = 9.9 nm which was lower than R_h = 14.5 nm whereas the distribution widths were comparable from both techniques. This is in

agreement with a core-shell structure of the nano-assemblies, *i.e.* a denser polymer core and a corona made of hydrated PMeOx chains. Indeed, the hydrodynamic radius includes the solvent displaced by the nano-object whereas SANS should probe only the dense core, the scattering length density of the hydrated corona layer being very close to the one of D_2O. It is thus reasonable to assume that R_{SANS} corresponds to the core radius.

It was possible to calculate the contour length of each block L_C(PLA) and L_C(PMeOx), to verify the possibility of a micellar core-shell structure by determining the maximum radius that could have a core only made of PLA and the maximum extension of a PMeOx external layer (equation 5):

$$L_c(\mathrm{PLA}) = a_{PLA} \times DP_{PLA} \quad \text{and} \quad L_c(\mathrm{PMeOx}) = a_{PMeOx} \times DP_{PMeOx} \tag{5}$$

In which DP_{PLA} and DP_{PMeOx} are the degrees of polymerization of PLA and PMeOx respectively, and a_{PLA} and a_{PMeOx} are the lengths of a repeating unit in PLA and PMeOx, both approximated to 3.5 Å (0.35 nm). Values are reported in Table 3. In all cases, R_{SANS} was lower than L_C(PLA). Moreover, the thickness of the corona layer, roughly estimated from the difference between R_h and R_{SANS} were also always lower than L_C(PMeOx). The aggregates had thus likely a micellar core-shell structure with a core made of PLA blocks' self-assembly and a corona of non-extended PMeOx.

The results showed that with the same size of the hydrophilic PMeOx block, the core radius increased with an increase of the hydrophobic PLA block polymer length, from 9.9 nm for $PMeOx_{2200}$-*b*-PLA_{2800} to 16.7 nm for $PMeOx_{2200}$-*b*-PLA_{5200}. Moreover, the thickness of the PMeOx shell increased with the PMeOx length, as roughly represented by the difference R_h - R_{SANS} which was about 5.0 – 7.0 nm for $PMeOx_{2200}$ and 16.0 nm for $PMeOx_{5200}$. These observations are consistent with previous studies on other linear amphiphilic diblock copolymers.[46]

In order to demonstrate the coherence of this analysis, aggregation numbers N_{agg} were estimated assuming that the core was made of only PLA blocks and contained no solvent (equation 6):

$$N_{agg} = \frac{N_A d}{\overline{M_n}_{PLA}} \left(\frac{4\pi r_{core}^3}{3}\right) \quad (6)$$

Where $\overline{M_n}_{PLA}$ was the PLA number-average molecular mass obtained by ^{1}H NMR, N_A the Avogadro number, d the density of the PLA block equal to 1.25 g.cm^{-3} and r_{core} estimated as R_{SANS}.

The data are presented in Table 3. N_{agg} are ranging from 500 to 2800. These are relatively high values compared to the ones reported for micellar surfactants (less than few hundred).[47] The unusually high N_{agg} values were mainly due to the formation of "irregular" micelles made of a frozen PLA core. However, these values were always lower than the maximum N_{agg} values calculated for a given PLA block and obtained by replacing r_{core} by Lc(PLA) in equation 6. (N_{agg}) max were equal to 1700 and 10600 for PLA blocks of 2800 and 5200 g.mol^{-1} respectively. More quantitatively, N_{agg} decreased when the hydrophilic weight fraction *f* increased.

Discher [48,49] proposed an unified empirical rule based on the ratio *f* of the molecular mass of the hydrophilic part to the total molecular mass: polymersomes are generally observed in the *f* range 25 % - 40 %, worm like micelles in the *f* range 40 % - 50 %, and spherical micelles for higher *f* values. Several authors verified this rule and reported the formation of core-shell micellar structures for PMeOx-based diblock copolymers in which the hydrophilic weight ratio *f* was larger than 50 %[26,50] but also for triblock copolymers with a hydrophobic middle block. For instance the self-assembly of poly(2-methyl-2-oxazoline)-*b*-poly(tetrahydrofuran)-*b*-poly(2-methyl-2-oxazoline) (PMeOx-*b*-PTHF-*b*-PMeOx) amphiphilic triblock copolymers was previously reported by Rasolonjatovo *et al.*,[24] they showed the increase of the

hydrodynamic radius of micelles when the PMeOx length increased and the PTHF length remained constant. On the other hand, well defined polymersome morphologies have been obtained with PMeOx-*b*-PDMS diblock copolymers as well as PMeOx-*b*-PDMS-*b*-PMeOx triblock copolymers within the expected hydrophilic weight ratio range, between 20 and 30 %.[23,51] When the hydrophobic middle block (poly(2-phenyl-2-oxazoline)) was glassy, polymersomes were also observed, for a hydrophilic weight ratio of 50 % but in coexistence with micelles.[52]

Le Meins *et al.*[53] recalled that for polymers, the obtained morphologies not only results from geometrical parameters but an entropy and enthalpy loss must be taken into account during the self-assembling process. In our case, multiple morphologies were expected as *f* was varied between 30 and 66 %. However, only the spherical micelles morphologies were clearly identified in this work. The other morphologies (vesicles, wormlike micelles) were not reached. This could be due to the kinetically trapped system led by the kinetic of solvent diffusion faster than the kinetics of self-assembly (by nanoprecipitation), leading to frozen morphologies. Similar findings have also been reported of PEG-*co*-PLA copolymers with *f* ratio close to 0.2 using a flash nanoprecipitation[46] method whereas micrometric sized vesicles where observed using a slow water dissolution process with *f* in the range 0.2 – 0.42.[54] This phenomenon confirms that even if it is reported that the morphologies are in part predetermined by the macromolecular composition, the material morphology can also be controlled by the self-assembly process used.[55,56]

Self-assembly study of the triblock copolymers

Next we studied the self-assembly behavior of the ABA triblock copolymers, in a B-selective solvent. For this purpose, six copolymers with different compositions were synthesized: three

copolymers having a hydrophilic middle block of 8.2×10^3 g.mol^{-1}: PLA$_{1200}$-*b*-PMeOx$_{8200}$-*b*-PLA$_{1200}$ (f = 77 %), PLA$_{2200}$-*b*-PMeOx$_{8200}$-*b*-PLA$_{2200}$ (f = 67 %), PLA$_{4200}$-*b*-PMeOx$_{8200}$-*b*-PLA$_{4200}$ (f = 50 %) and three copolymers having a hydrophilic middle block of 2.2×10^3 g.mol^{-1}: PLA$_{1200}$-*b*-PMeOx$_{2200}$-*b*-PLA$_{1200}$ (f = 48 %), PLA$_{2200}$-*b*-PMeOx$_{2200}$-*b*-PLA$_{2200}$ (f = 34 %), PLA$_{4200}$-*b*-PMeOx$_{2200}$-*b*-PLA$_{4200}$ (f = 21 %). Self-assembly of PLA-*b*-PMeOx-*b*-PLA triblock copolymers was triggered by nanoprecipitation in water from ACN solution but also by dialysis from ACN (see experimental part) for some of the samples, a slower solvent mixing process, in order to compare nano-structures obtained from both techniques.

The suspensions were firstly characterized by DLS at 173°. The results showed nano-objects with hydrodynamic radii between 14 nm and 30 nm depending on the composition as well as objects of several hundred nanometers (as shown in the Figure 7.A for the distribution based on PLA$_{2200}$-b-PMeOx$_{8200}$-*b*-PLA$_{2200}$ by nanoprecipitation).

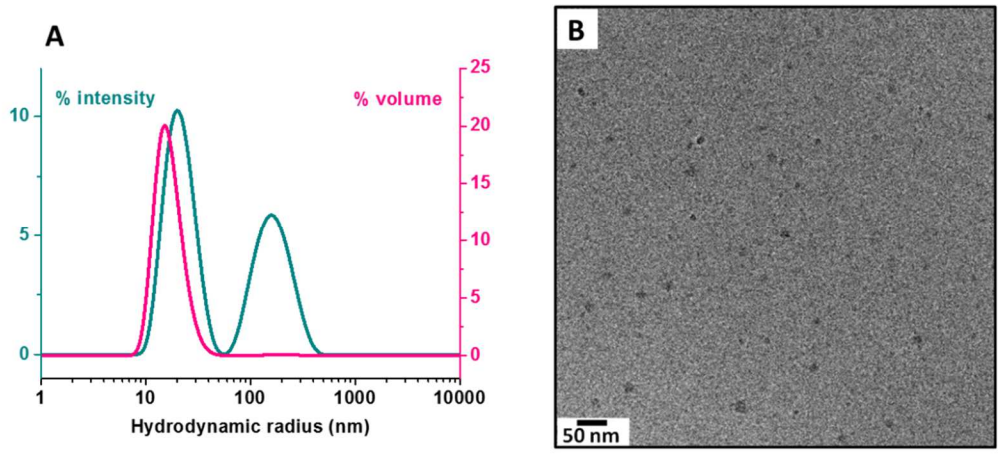

Figure 7. (A) DLS size distribution and (B) cryo-TEM micrograph of nano-objects of PLA$_{2200}$-*b*-PMeOx$_{8200}$-*b*-PLA$_{2200}$ (f = 67 %) obtained by nanoprecipitation.

The distribution widths σ_{DLS} are high, of the order of 0.6 and in the same range as for the diblock copolymers, because of the bimodal size distribution (only in intensity, volume size distributions showed a unimodal distribution). R_h and σ_{DLS} values are reported in Table 4.

1 It should be outlined that the contribution of the large size aggregates on the intensity signal
2 is somewhat larger in the case of the samples obtained by the dialysis method. Moreover, a
3 discreet signal corresponding to these large aggregates is persistent on the volume signal
4 (Figure 8, PLA_{2200}-b-$PMeOx_{2200}$-*b*-PLA_{2200}).

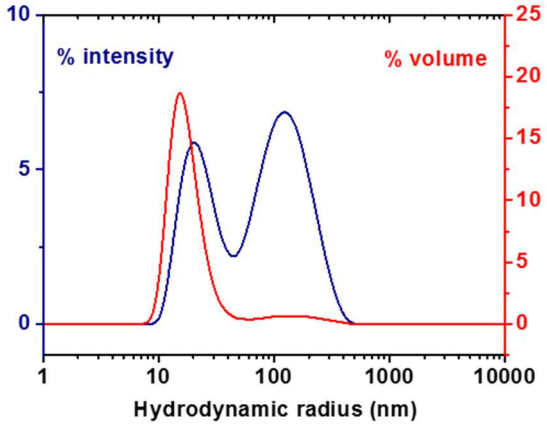

5

6 Figure 8. DLS size distribution of nano-objects of PLA_{2200}-*b*-$PMeOx_{8200}$-*b*-PLA_{2200} (f = 67
7 %) obtained by dialysis.

8

9 The intensity representation gives a strong importance to the aggregates, so we chose to
10 retain the R_h value in volume distribution in order to characterize the sizes of the majority of
11 objects.
12 The cryo-TEM micrographs of the suspension based on PLA_{2200}-*b*-$PMeOx_{8200}$-*b*-PLA_{2200}
13 copolymer (Figure 7.B) showed spherical structures with an average radius of 9.5 nm which
14 was smaller than the hydrodynamic radius obtained by DLS (17.0 nm). This can be explained
15 by the influence of the largest structures on the hydrodynamic diameter obtained by DLS, but
16 also one should consider that hydrodynamic diameters take into account the solvent displaced
17 by the nano-objects and this could result in an overestimate of the size.

The self-assemblies from triblock copolymers were characterized by SANS in D_2O at 1 $g.L^{-1}$ and at room temperature. Figure 9 and Figure S7 show the plots of the scattered intensity as a function of q from the different samples obtained by nanoprecipitation and dialysis respectively. For better visibility, intensity was multiplied by a power of 10 on the graph.

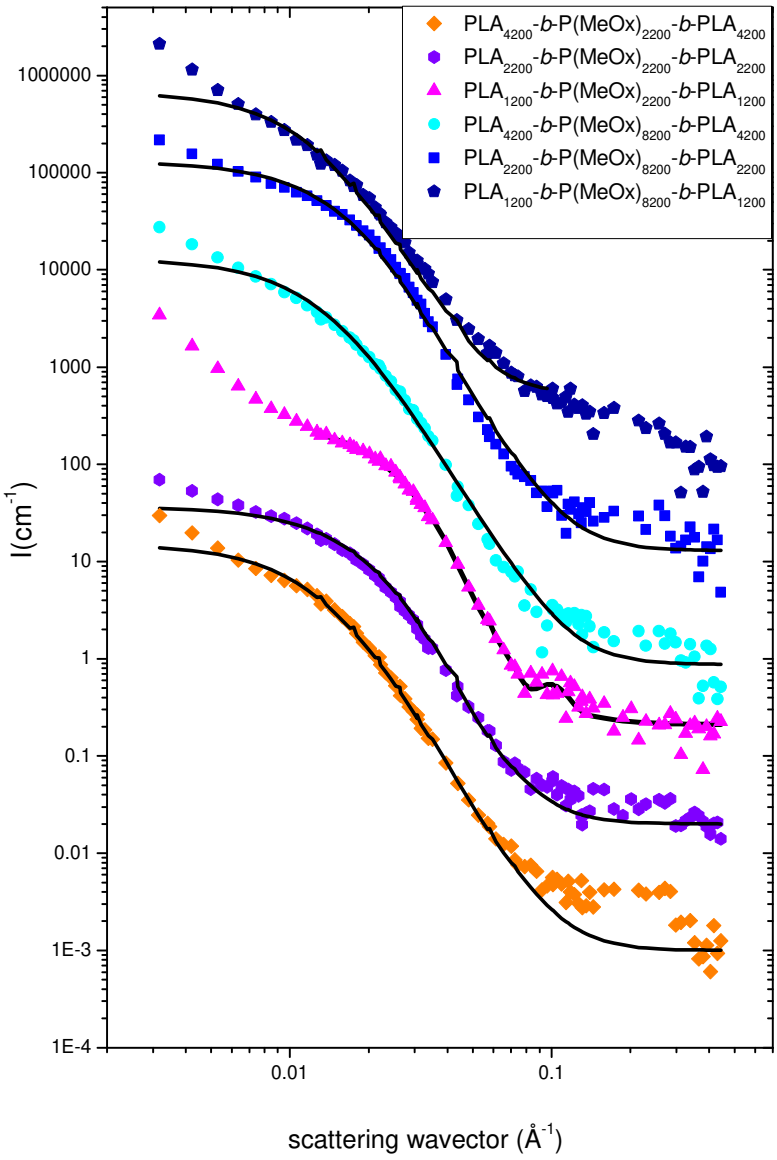

Figure 9. Scattered intensity as a function of scattering vector q for nano-objects of PLA-*b*-PMeOx-*b*-PLA obtained by nanoprecipitation (the solid black lines are the fitting curves).

Similar to the SANS results obtained for the diblocks, the six curves were characterized by a variation in q^{-4} in the intermediate q value regime ($2.0\times10^{-2} < q$ (Å^{-1}) $< 8.0\times10^{-2}$) that may correspond to a compact structure. While for larger values of q ($8.0\times10^{-2} < q$ (Å^{-1}) $< 4.4\times10^{-1}$), the decrease of log *I* was less abrupt. This variation might be characteristic of an interface coated with hydrated polymer chains. However, the absence of a variation in q^{-2} was due to the impossibility to subtract more incoherent from the solvent.

The low q behavior ($3.0\times10^{-3} < q$ (Å^{-1}) $< 2.0\times10^{-2}$) was quite different from the one observed for the diblock copolymers. In all cases, there was an intensity increase as q decreased which should be characteristic of an aggregation phenomenon. The self-assemblies were thus made of finite size aggregates, as can be extrapolated from the combination of DLS, cryo-TEM and SANS results.

Table 4. Characteristics of PLA-*b*-PMeOx-*b*-PLA nano-objects

Copolymers	Method[(a)]	*f* (%)	R_h [(b)] (nm)	σ_{DLS}[(a)]	R_{SANS} or R^c_{SANS}, δ^1_{SANS}, δ^2_{SANS} [(c)] (nm)	σ_{SANS} or σ^c_{SANS}, σ^1_{SANS}, σ^2_{SANS} [(c)]	N_{agg}[(d)]
PLA_{4200}-*b*-$PMeOx_{2200}$-*b*-PLA_{4200}	1	21	31.0	0.48	6.4	0.42	98
PLA_{2200}-*b*-$PMeOx_{2200}$-*b*-PLA_{2200}	1	34	15.0	0.73	6.9	0.33	242
PLA_{1200}-*b*-$PMeOx_{2200}$-*b*-PLA_{1200}	1	48	14.5	0.57	3.4/1.5/1.7	0.25/0.4/0.4	275
PLA_{4200}-*b*-$PMeOx_{8200}$-*b*-PLA_{4200}	1	50	31.0	0.53	6.5	0.45	109
PLA_{2200}-*b*-$PMeOx_{8200}$-*b*-PLA_{2200}	1	67	17.0	0.68	8.2	0.31	410
PLA_{1200}-*b*-$PMeOx_{8200}$-*b*-PLA_{1200}	1	77	-*	-*	6.0	0.55	283
PLA_{4200}-*b*-$PMeOx_{2200}$-*b*-PLA_{4200}	2	21	25.0	0.63	11.5	0.35	593
PLA_{2200}-*b*-$PMeOx_{2200}$-*b*-PLA_{2200}	2	34	16.0	0.60	6.9	0.45	244
PLA_{2200}-*b*-$PMeOx_{8200}$-*b*-PLA_{2200}	2	67	18.0	0.69	10.4	0.17	830

(a) Method 1 is nanoprecipitation, method 2 is dialysis

(b) Hydrodynamic radii (R_h) and σ_{DLS} values determined by DLS

(c) Determined by fitting the SANS curves using a polydisperse sphere or a core multishell model.

(d) Aggregation number.

*These values are not accessible by DLS measurement, the correlogram is not correct due to the large presence of the aggregates

The SANS data were fitted and the traces of the fits obtained are in black in Figure 9. A polydisperse sphere model was used in most cases. As was highlighted in the diblock self-assembly study, SANS probes mainly the dense PLA core because the hydrated PMeOx corona has a contrast length density close to the one of D_2O. Consequently, the fits parameters, R_{SANS} and σ_{SANS}, are thus characteristic of the core radius of the micelles. R_{SANS} were in a close range 6.0 – 8.2 nm for the nanoprecipitation method and 6.9 – 11.5 nm for the dialysis method, without a marked dependence upon the PLA chain length. Interestingly, R_{SANS} for the triblocks were smaller than the ones determined for the diblocks (9.5- 16.7 nm) whereas R_h of the triblocks had comparable values to the ones of the diblocks. One can notice that R_{SANS} were always lower than R_h as expected, the latter being sensitive to the hydrated micellar corona and to the aggregation phenomenon. Interestingly, for PLA_{1200}-*b*-$PMeOx_{2200}$-*b*-PLA_{1200}, a polydisperse core-multishell model was found to be the most appropriate model to fit the SANS data. It consists in a dense PLA core (ρ_{PLA}, R^c_{SANS} and σ^c_{SANS}), a hydrated shell (ρ_{D2O}, R^1_{SANS} and σ^1_{SANS}) and an external PLA shell (ρ_{PLA}, R^2_{SANS} and σ^2_{SANS}). Again, in this case, the total radius (R^2_{SANS}= 7.1 nm) was in the same range as for the other triblocks and much lower than R_h.

In all the cases, the aggregation number has been deduced from a similar calculation as for the diblock copolymers (equation 6). In the case of the analysis by a core-multishell model, the term $4/3\pi(r_c)^3$ has been replaced in the same equation by the total volume of the PLA domains (in the core and in the shell). As was expected from the values of R_{SANS}, N_{agg} were smaller than the ones estimated for the diblock copolymers. Values depended on the preparation method. N_{agg} were in the range 100- 400 for the nanoprecipitated samples and were generally larger for the dialyzed samples 240-830.

The dialysis method brought about similar results as from the nanoprecipitation method, except that R_{SANS}, N_{agg} were generally larger in the former method. Figure 10 shows the overlay of the SANS plots obtained from the 2 methods for a same sample (PLA_{2200}-*b*-$PMeOx_{2200}$-*b*-PLA_{2200}).

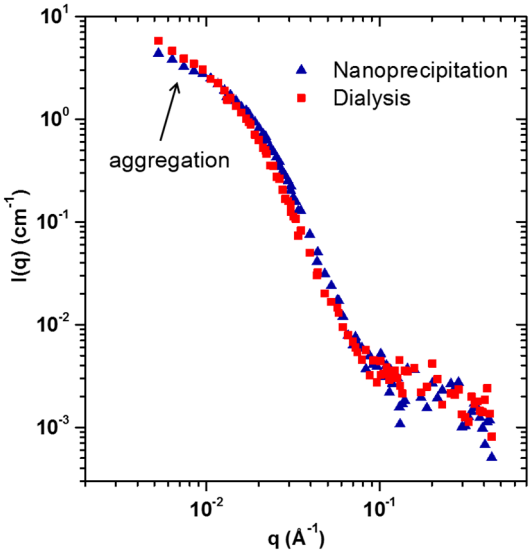

Figure 10. Scattered intensity as a function of q for nano-objects of PLA_{2200}-*b*-$PMeOx_{2200}$-*b*-PLA_{2200} (f = 34 %) obtained by nanoprecipitation and by dialysis.

Whereas these two samples showed very similar SANS signals, the aggregation was stronger in the sample prepared from dialysis method as the scattered intensity at low q increased more steeply. Indeed, when the self-assembly took place more slowly, here *via* a dialysis process, the micelles which were close enough, could form more bridges between them.

The self-assembly of triblock copolymers PLA-*b*-PMeOx-*b*-PLA, by two relatively rapid processes compare to other common methods such as direct solubilization or slow addition of water in organic solution for example, thus allowed the formation of micelles. Average

aggregate radii were in the range 15.0 – 30.0 nm although DLS highlighted the presence of a small proportion of larger objects of several hundred nanometers. The SANS and cryo-TEM measurements revealed the compact structure of the micellar cores and SANS showed their aggregation into connected structures. Several authors have reported upon the self-assemblies of ABA triblock copolymers in a B-selective solvent.[57,58] Two types of association mechanisms were described: (i) a closed association mechanism leading to flower-like micelles where the hydrophilic middle block is looped at the outer rim of the micelle, the core being composed of the hydrophobic block; and (ii) an open association mechanism with the formation of loose aggregates. Formation of micelles was reported using a crystalline PLLA block in PLLA-*b*-PEtOx-*b*-PLLA by Hsiue and co-workers[59]. In the case of the same amorphous PLA blocks as in the present study, a closed association mechanism was also reported as micelles were detected and analyzed in PLA-*b*-PEO-*b*-PLA copolymers of *f* ratio larger than 0.5.[57,58] The results of Bhatia and co-workers were also in good agreement with the formation of flower-like micelles where the core sizes and aggregation numbers increased with the PLA molecular mass. It should be noted that the core sizes were on the same order as for the micelles of this study (for comparable PLA number-average molecular mass). Moreover, networks of bridged micelles were reported as the concentration was increased above 100 $g.L^{-1}$ but there was no report of the formation aggregates of bridged micelles at concentration as low as 1 $g.L^{-1}$ as in the present work.

As for the diblocks, there is the question of the micelles' morphology as a function of the *f* parameter . Additionnaly to the geometrical and energetic parameters already mentioned for the diblocks, one must take into account the entropy loss associated to the looping of the middle block. This last constraint might be less strong when the middle block has a larger molecular mass. In the experiments, there were two series of triblock copolymers, three copolymer samples with a short PMeOx block (2200 $g.mol^{-1}$) and three other samples with a

PMeOx block more than three times longer (8200 g.mol^{-1}). As *f* is larger than 50 % for these last three copolymers, spherical micelles were expected, and the results were in good agreement whatever the preparation method chosen. The lower core radius, in comparison to the ones of the diblocks, could be attributed to the looping penalty of the middle block. The series with shorter PMeOx block had *f* values in a 21-48 % range. For PLA_{4200}-*b*-$PMeOx_{2200}$-*b*-PLA_{4200}, *f* = 21 %, spherical micellar morphologies were obtained using nanoprecipitation and dialysis method. This is in good agreement with the Discher morphology rules [48,49]. For the two other triblock copolymers with *f* values of 34 and 48 %, vesicular morphologies could be expected following the same rule. A core-multishell morphology have been detected for PLA_{1200}-*b*-$PMeOx_{2200}$-*b*-PLA_{1200} using the nanoprecipitation preparation method and appearing as a shoulder in the intermediate q-range of the plot. This morphology might exist for other samples (such as samples with *f* = 34%) but could not be always detected by SANS due to smoothing polydispersity effects. The core-multishell morphologies were not observed for the diblocks, neither from the SANS plots nor from the cryo-TEM pictures. In the case of the triblocks, the formation of core-multishell structures should be favoured because of the looping penalty of the short PMeOx block.

The following association behavior is thus proposed as a function of the parameter *f* in Scheme 2. Whatever the value of *f*, bridged micelles of finite size were formed but those might coexist with isolated micelles which have not been represented in Scheme 2 for the sake of simplicity. The micellar core may have an inner structure depending on *f* as well as the middle block molecular mass. Indeed, for very close *f* values, 48 and 50 %, core-multishell and core-shell structures were respectively observed due to the PMeOx block length increase.

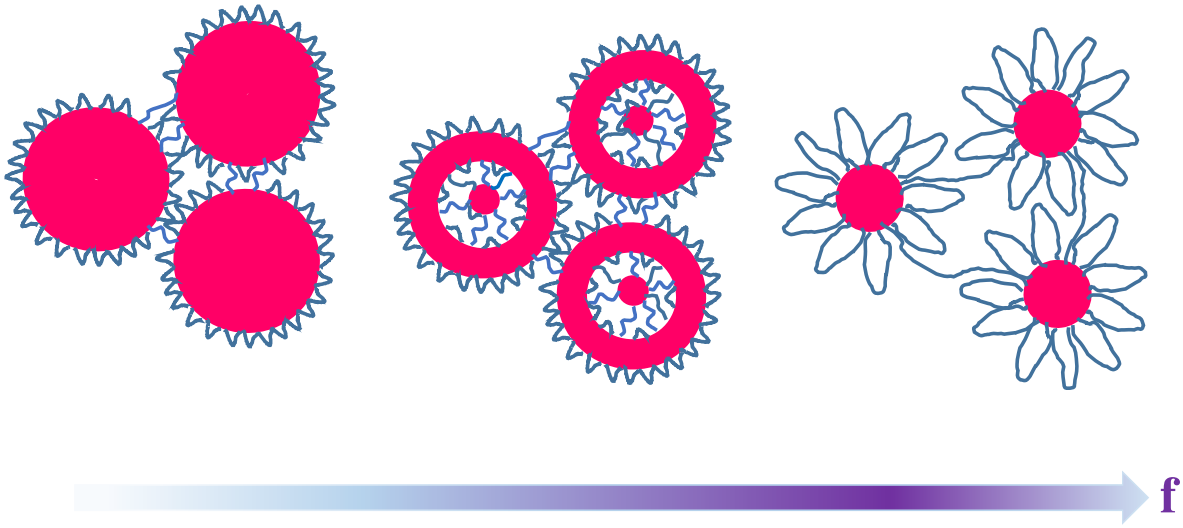

Scheme 2: Association scheme of the triblock copolymers as a function of the hydrophilic ratio *f*. Isolated micelles may coexist with bridged micelles in each case but for simplicity it has not been drawn.

However, the technique of self-assembly used has a great influence on the self-assembly process. Systematic experiments provided information about the location of the "Ouzo domain", in which only nanoparticles are obtained, and identified the parameters controlling the size, polydispersity and the crystallinity of nanoparticles.[60] The copolymer composition has a significant influence but the mixing time of the organic solution containing the amphiphilic copolymer with the aqueous phase is a parameter of first importance. When the kinetics of self-assembly is slown down by a rapid solvent mixing, here by nanoprecipitation or dialysis, copolymers do not have enough mobility during the self-assembly to reach the most stable morphology, the system is trapped under a metastable structure, often of reduced mean size, as the polydisperse core-multishell and micellar structures obtained in this study. Consequently, these structures were obtained by the combination of parameters, among them, the copolymer characteristics and the used self-assembly routes.

Conclusion

Novel well defined diblock and triblock amphiphilic copolymers PMeOx-*b*-PLA and PLA-*b*-PMeOx-*b*-PLA were successfully synthesized *via* CROP and copper-catalyzed Huisgen 1,3-dipolar cycloaddition. In that way, two series of copolymers with varying PLA as well as PMeOx chain length were prepared allowing reaching hydrophilic weight ratio (*f*) in a wide range (21 to 77 %). These copolymers were self-assembled in water *via* solvent displacement methods and in all cases, "irregular" micelles with quite high aggregation numbers where obtained due to the frozen nature of the PLA blocks. For the diblock copolymers, core-shell micellar structures with a dense PLA core and a hydrated PMeOx shell were obtained in the whole range of *f* values. Although vesicular structures were reported in parent diblock copolymers such as PEO-*b*-PLA, their absence in the present study was attributed to the fast preparation method by nanoprecipitation. An original association behavior was evidenced for the triblock copolymers. At concentration as low as 1 $g.L^{-1}$, they formed spherical micelle-like structure with a few aggregates of finite sizes made of bridged micelles, the micelles being connected by some of the PLA end-blocks. This finding has been reported for the parent PLA-*b*-PEO-*b*-PLA copolymers but it occurred only at much larger concentrations than in the present study. Moreover, the micelles displayed original nanostructures with the formation of core-multishell structures in a specific range of *f* values (close to 48 %) never reported for this kind of triblock copolymers. This process could be favored to reduce the entropy loss coming from the looping of the PMeOx middle blocks when forming simple flower-like micelles. The amphiphilic copolymers of this study displayed a rich variety of controlled self-assembled morphologies which could be promising candidates for drug delivery applications.

Acknowledgement

We are grateful to Sena Hamadi for SEC analysis and ICP-OES measurements as well as Mohamed Guerrouache for Raman spectroscopy. We would like to thank the LLB-Orphée large-scale facility for giving us access to SANS measurements and Fabrice Cousin for discussions and help during experiments. We would like to thank Nathalie Jarroux, Laboratoire Analyse et Modélisation pour la Biologie et l'Environnement (LAMBE), Université d'Evry Val d'Essonne for her help for SEC analysis in DMF.

REFERENCES

(1) Adams, M. L.; Lavasanifar, A.; Kwon, G. S. Amphiphilic block copolymers for drug delivery. *Journal of pharmaceutical sciences* **2003**, *92*, 1343-1355.

(2) Kwon, G. S.; Kataoka, K. Block copolymer micelles as long-circulating drug vehicles. *Advanced drug delivery reviews* **1995**, *16*, 295-309.

(3) Kataoka, K.; Harada, A.; Nagasaki, Y. Block copolymer micelles for drug delivery: design, characterization and biological significance. *Advanced drug delivery reviews* **2012**, *64*, 37-48.

(4) Biswas, S.; Kumari, P.; Lakhani, P. M.; Ghosh, B. Recent advances in polymeric micelles for anti-cancer drug delivery. *European Journal of Pharmaceutical Sciences* **2016**, *83*, 184-202.

(5) Kabanov, A. V.; Batrakova, E. V.; Melik-Nubarov, N. S.; Fedoseev, N. A.; Dorodnich, T. Y.; Alakhov, V. Y.; Chekhonin, V. P.; Nazarova, I. R.; Kabanov, V. A. A new class of drug carriers: micelles of poly (oxyethylene)-poly (oxypropylene) block copolymers as microcontainers for drug targeting from blood in brain. *Journal of Controlled Release* **1992**, *22*, 141-157.

(6) Meng, X.; Liu, J.; Yu, X.; Li, J.; Lu, X.; Shen, T. Pluronic F127 and D-α-Tocopheryl Polyethylene Glycol Succinate (TPGS) Mixed Micelles for Targeting Drug Delivery across The Blood Brain Barrier. *Scientific Reports* **2017**, *7*, 2964.

(7) Scholz, C.; Iijima, M.; Nagasaki, Y.; Kataoka, K. A novel reactive polymeric micelle with aldehyde groups on its surface. *Macromolecules* **1995**, *28*, 7295-7297.

(8) Nagasaki, Y.; Okada, T.; Scholz, C.; Iijima, M.; Kato, M.; Kataoka, K. The reactive polymeric micelle based on an aldehyde-ended poly (ethylene glycol)/poly (lactide) block copolymer. *Macromolecules* **1998**, *31*, 1473-1479.

(9) Osada, K.; Christie, R. J.; Kataoka, K. Polymeric micelles from poly (ethylene glycol)–poly (amino acid) block copolymer for drug and gene delivery. *Journal of The Royal Society Interface* **2009**, *6*, S325-S339.

(10) Lin, J.; Zhu, G.; Zhu, X.; Lin, S.; Nose, T.; Ding, W. Aggregate structure change induced by intramolecular helix–coil transition. *Polymer* **2008**, *49*, 1132-1136.

(11) Priftis, D.; Leon, L.; Song, Z.; Perry, S. L.; Margossian, K. O.; Tropnikova, A.; Cheng, J.; Tirrell, M. Self-Assembly of α-Helical Polypeptides Driven by Complex Coacervation. *Angewandte Chemie* **2015**, *127*, 11280-11284.

(12) Armstrong, J. K.; Hempel, G.; Koling, S.; Chan, L. S.; Fisher, T.; Meiselman, H. J.; Garratty, G. Antibody against poly (ethylene glycol) adversely affects PEG-asparaginase therapy in acute lymphoblastic leukemia patients. *Cancer* **2007**, *110*, 103-111.

(13) Sherman, M. R.; Saifer, M. G.; Perez-Ruiz, F. PEG-uricase in the management of treatment-resistant gout and hyperuricemia. *Advanced drug delivery reviews* **2008**, *60*, 59-68.

(14) Leger, R.; Arndt, P.; Garratty, G.; Armstrong, J.; Meiselman, H.; Fisher, T. In *Tilte*2001; AMER ASSOC BLOOD BANKS 8101 GLENBROOK RD, BETHESDA, MD 20814-2749 USA.

(15) Armstrong, J.; Leger, R.; Wenby, R.; Meiselman, H.; Garratty, G.; Fisher, T. In *Tilte*2003; AMER SOC HEMATOLOGY 1900 M STREET. NW SUITE 200, WASHINGTON, DC 20036 USA.

(16) Barz, M.; Luxenhofer, R.; Zentel, R.; Vicent, M. J. Overcoming the PEG-addiction: well-defined alternatives to PEG, from structure–property relationships to better defined therapeutics. *Polymer Chemistry* **2011**, *2*, 1900-1918.

(17) Gubarev, A. S.; Monnery, B. D.; Lezov, A. A.; Sedlacek, O.; Tsvetkov, N. V.; Hoogenboom, R.; Filippov, S. K. Conformational properties of biocompatible poly (2-ethyl-2-oxazoline) s in phosphate buffered saline. *Polymer Chemistry* **2018**, *9*, 2232-2237.

(18) Hoogenboom, R. Poly (2-oxazoline) s: a polymer class with numerous potential applications. *Angewandte Chemie International Edition* **2009**, *48*, 7978-7994.

(19) Adams, N.; Schubert, U. S. Poly (2-oxazolines) in biological and biomedical application contexts. *Advanced drug delivery reviews* **2007**, *59*, 1504-1520.

(20) Luxenhofer, R.; Han, Y.; Schulz, A.; Tong, J.; He, Z.; Kabanov, A. V.; Jordan, R. Poly (2-oxazoline) s as Polymer Therapeutics. *Macromolecular rapid communications* **2012**, *33*, 1613-1631.

(21) Luxenhofer, R.; Sahay, G.; Schulz, A.; Alakhova, D.; Bronich, T. K.; Jordan, R.; Kabanov, A. V. Structure-property relationship in cytotoxicity and cell uptake of poly (2-oxazoline) amphiphiles. *Journal of Controlled Release* **2011**, *153*, 73-82.

(22) Bauer, M.; Lautenschlaeger, C.; Kempe, K.; Tauhardt, L.; Schubert, U. S.; Fischer, D. Poly (2-ethyl-2-oxazoline) as Alternative for the Stealth Polymer Poly (ethylene glycol): Comparison of in vitro Cytotoxicity and Hemocompatibility. *Macromolecular bioscience* **2012**, *12*, 986-998.

(23) Nardin, C.; Hirt, T.; Leukel, J.; Meier, W. Polymerized ABA triblock copolymer vesicles. *Langmuir* **2000**, *16*, 1035-1041.

(24) Rasolonjatovo, B.; Gomez, J.-P.; Même, W.; Gonçalves, C.; Huin, C. c.; Bennevault-Celton, V. r.; Le Gall, T.; Montier, T.; Lehn, P.; Cheradame, H.; Midoux, P.; Guégan, P. Poly (2-methyl-2-oxazoline)-b-poly (tetrahydrofuran)-b-poly (2-methyl-2-oxazoline) Amphiphilic Triblock Copolymers: Synthesis, Physicochemical Characterizations, and Hydrosolubilizing Properties. *Biomacromolecules* **2015**, *16*, 748-756.

(25) Kempe, K.; Hoogenboom, R.; Hoeppener, S.; Fustin, C.-A.; Gohy, J.-F.; Schubert, U. S. Discovering new block terpolymer micellar morphologies. *Chemical Communications* **2010**, *46*, 6455-6457.

(26) Bonné, T. B.; Lüdtke, K.; Jordan, R.; Štěpánek, P.; Papadakis, C. M. Aggregation behavior of amphiphilic poly (2-alkyl-2-oxazoline) diblock copolymers in aqueous solution studied by fluorescence correlation spectroscopy. *Colloid and Polymer Science* **2004**, *282*, 833-843.

(27) Krumm, C.; Fik, C. P.; Meuris, M.; Dropalla, G. J.; Geltenpoth, H.; Sickmann, A.; Tiller, J. C. Well-Defined Amphiphilic Poly (2-oxazoline) ABA-Triblock Copolymers and Their Aggregation Behavior in Aqueous Solution. *Macromolecular rapid communications* **2012**, *33*, 1677-1682.

(28) Anderson, J. M.; Shive, M. S. Biodegradation and biocompatibility of PLA and PLGA microspheres. *Advanced drug delivery reviews* **1997**, *28*, 5-24.

(29) Ramot, Y.; Haim-Zada, M.; Domb, A. J.; Nyska, A. Biocompatibility and safety of PLA and its copolymers. *Advanced drug delivery reviews* **2016**, *107*, 153-162.

(30) Riley, T.; Govender, T.; Stolnik, S.; Xiong, C.; Garnett, M.; Illum, L.; Davis, S. Colloidal stability and drug incorporation aspects of micellar-like PLA–PEG nanoparticles. *Colloids surfaces B: Biointerfaces* **1999**, *16*, 147-159.

(31) Riley, T.; Stolnik, S.; Heald, C.; Xiong, C.; Garnett, M.; Illum, L.; Davis, S.; Purkiss, S.; Barlow, R.; Gellert, P. Physicochemical evaluation of nanoparticles assembled from Poly (lactic acid)− Poly (ethylene glycol)(PLA− PEG) block copolymers as drug delivery vehicles. *Langmuir* **2001**, *17*, 3168-3174.

(32) Salem, A.; Cannizzaro, S.; Davies, M.; Tendler, S.; Roberts, C.; Williams, P.; Shakesheff, K. Synthesis and characterisation of a degradable poly (lactic acid)− poly (ethylene glycol) copolymer with biotinylated end groups. *Biomacromolecules* **2001**, *2*, 575-580.

(33) Riley, T.; Heald, C.; Stolnik, S.; Garnett, M.; Illum, L.; Davis, S.; King, S.; Heenan, R.; Purkiss, S.; Barlow, R. Core− shell structure of PLA− PEG nanoparticles used for drug delivery. *Langmuir* **2003**, *19*, 8428-8435.

(34) Wang, C. H.; Hsiue, G. H. Synthesis and characterization of temperature-and pH-sensitive hydrogels based on poly (2-ethyl-2-oxazoline) and poly (D, L-lactide). *Journal of Polymer Science Part A: Polymer Chemistry* **2002**, *40*, 1112-1121.

(35) Decuzzi, P.; Godin, B.; Tanaka, T.; Lee, S.-Y.; Chiappini, C.; Liu, X.; Ferrari, M. Size and shape effects in the biodistribution of intravascularly injected particles. *Journal of Controlled Release* **2010**, *141*, 320-327.

(36) Yang, Y.; Nie, D.; Liu, Y.; Yu, M.; Gan, Y. Advances in particle shape engineering for improved drug delivery. *Drug Discovery Today* **2018**.

(37) Yokoyama, M.; Miyauchi, M.; Yamada, N.; Okano, T.; Sakurai, Y.; Kataoka, K.; Inoue, S. Characterization and anticancer activity of the micelle-forming polymeric anticancer drug

adriamycin-conjugated poly (ethylene glycol)-poly (aspartic acid) block copolymer. *Cancer Research* **1990**, *50*, 1693-1700.

(38) Maeda, H.; Wu, J.; Sawa, T.; Matsumura, Y.; Hori, K. Tumor vascular permeability and the EPR effect in macromolecular therapeutics: a review. *Journal of Controlled Release* **2000**, *65*, 271-284.

(39) Kobayashi, H.; Watanabe, R.; Choyke, P. L. Improving conventional enhanced permeability and retention (EPR) effects; what is the appropriate target? *Theranostics* **2014**, *4*, 81.

(40) Matsumura, Y.; Maeda, H. A new concept for macromolecular therapeutics in cancer chemotherapy: mechanism of tumoritropic accumulation of proteins and the antitumor agent smancs. *Cancer research* **1986**, *46*, 6387-6392.

(41) Lav, T.-X.; Lemechko, P.; Renard, E.; Amiel, C.; Langlois, V.; Volet, G. Development of a new azido-oxazoline monomer for the preparation of amphiphilic graft copolymers by combination of cationic ring-opening polymerization and click chemistry. *Reactive and Functional Polymers* **2013**, *73*, 1001-1008.

(42) Le Fer, G.; Amiel, C.; Volet, G. Copolymers based on azidopentyl-2-oxazoline: synthesis, characterization and LCST behavior. *European Polymer Journal* **2015**, *71*, 523-533.

(43) Volet, G.; Lav, T. X.; Babinot, J.; Amiel, C. Click-Chemistry: An Alternative Way to Functionalize Poly (2-methyl-2-oxazoline). *Macromolecular Chemistry and Physics* **2011**, *212*, 118-124.

(44) Le Fer, G. l.; Le Cœur, C. m.; Guigner, J.-M.; Amiel, C.; Volet, G. l. Biocompatible Soft Nanoparticles with Multiple Morphologies Obtained from Nanoprecipitation of Amphiphilic Graft Copolymers in a Backbone-Selective Solvent. *Langmuir* **2017**, *33*, 2849-2860.

(45) Lepeltier, E.; Bourgaux, C.; Couvreur, P. Nanoprecipitation and the "Ouzo effect": Application to drug delivery devices. *Advanced drug delivery reviews* **2014**, *71*, 86-97.

(46) Szymusiak, M.; Kalkowski, J.; Luo, H.; Donovan, A. J.; Zhang, P.; Liu, C.; Shang, W.; Irving, T.; Herrera-Alonso, M.; Liu, Y. Core–Shell Structure and Aggregation Number of Micelles Composed of Amphiphilic Block Copolymers and Amphiphilic Heterografted Polymer Brushes Determined by Small-Angle X-ray Scattering. *ACS macro letters* **2017**, *6*, 1005-1012.

(47) Israelachvili, J. N.: *Intermolecular and surface forces*; Academic press, 2011.

(48) Discher, D. E.; Eisenberg, A. Polymer vesicles. *Science* **2002**, *297*, 967-973.

(49) Discher, D. E.; Ahmed, F. Polymersomes. *Annu. Rev. Biomed. Eng.* **2006**, *8*, 323-341.

(50) Ivanova, R.; Komenda, T.; Bonné, T. B.; Lüdtke, K.; Mortensen, K.; Pranzas, P. K.; Jordan, R.; Papadakis, C. M. Micellar Structures of Hydrophilic/Lipophilic and Hydrophilic/Fluorophilic Poly (2-oxazoline) Diblock Copolymers in Water. *Macromolecular Chemistry and Physics* **2008**, *209*, 2248-2258.

(51) Dieu, L.-H.; Wu, D.; Palivan, C. G.; Balasubramanian, V.; Huwyler, J. Polymersomes conjugated to 83-14 monoclonal antibodies: in vitro targeting of brain capillary endothelial cells. *European journal of pharmaceutics and biopharmaceutics* **2014**, *88*, 316-324.

(52) Krumm, C.; Fik, C. P.; Meuris, M.; Dropalla, G. J.; Geltenpoth, H.; Sickmann, A.; Tiller, J. C. J. M. r. c. Well-Defined Amphiphilic Poly (2-oxazoline) ABA-Triblock Copolymers and Their Aggregation Behavior in Aqueous Solution. **2012**, *33*, 1677-1682.

(53) Le Meins, J.-F.; Sandre, O.; Lecommandoux, S. Recent trends in the tuning of polymersomes' membrane properties. *The European Physical Journal E* **2011**, *34*, 14.

(54) Discher, D. E.; Ahmed, F. Polymersomes. *Annual Review of Biomedical Engineering* **2006**, *8*, 323-341.

(55) Huang, J.; Bonduelle, C.; Thévenot, J.; Lecommandoux, S. b.; Heise, A. Biologically active polymersomes from amphiphilic glycopeptides. *Journal of the American Chemical Society* **2011**, *134*, 119-122.

(56) Le Fer, G.; Portes, D.; Goudounet, G.; Guigner, J.-M.; Garanger, E.; Lecommandoux, S. Design and self-assembly of PBLG-b-ELP hybrid diblock copolymers based on synthetic and elastin-like polypeptides. *Organic and biomolecular chemistry* **2017**, *15*, 10095-10104.

(57) Liu, T.; Kim, K.; Hsiao, B. S.; Chu, B. Regular and irregular micelles formed by A LEL triblock copolymer in aqueous solution. **2004**, *45*, 7989-7993.
(58) Agrawal, S. K.; Sanabria-DeLong, N.; Tew, G. N.; Bhatia, S. R. Structural Characterization of PLA− PEO− PLA Solutions and Hydrogels: Crystalline vs Amorphous PLA Domains. **2008**, *41*, 1774-1784.
(59) Wang, C.-H.; Hsiue, G.-H. New amphiphilic poly (2-ethyl-2-oxazoline)/poly (L-lactide) triblock copolymers. *Biomacromolecules* **2003**, *4*, 1487-1490.
(60) Pucci, C.; Cousin, F.; Dole, F.; Chapel, J.-P.; Schatz, C. Impact of the formulation pathway on the colloidal state and crystallinity of poly-ε-caprolactone particles prepared by solvent displacement. *Langmuir* **2018**, *34*, 2531-2542.

Graphical abstract